Monitoring Mobility in the Early Steps of Unfolding: The Case of Oxidized Cytochrome b_5 in the Presence of 2 M Guanidinium Chloride†

Fabio Arnesano, Lucia Banci, Ivano Bertini,* Dionysios Koulougliotis,‡ and Alessandro Monti

CERM and Department of Chemistry, University of Florence, Sesto Fiorentino, Italy

Received December 1, 1999; Revised Manuscript Received April 10, 2000

ABSTRACT: A Model-Free analysis of the ^{15}N relaxation properties of oxidized cytochrome b_5, a heme-containing electron-transfer protein, has been performed in 2 M guanidinium chloride (GdmCl), i.e., just before the heme is released by the action of denaturant. This analysis provides information on the mobility in the nano- to picosecond time range. A parallel study on the motions in the milli- to microsecond time scale has also been performed by analyzing rotating-frame ^{15}N relaxation rates. The protein contains a 60:40 ratio of two conformers (A and B) differing for the rotation of the heme group around the $\alpha-\gamma$ meso axis. The effect of denaturant has been followed for both species, and the mobility properties have been compared with the analogous information in the absence of denaturant. To complete the picture, we also performed ^{15}N relaxation measurements and the Model-Free analysis of the native B form, whereas data on the A form [Dangi, B., Sarma, S., Yan, C., Banville, D. L., Guiles, R. D. (1998) *J. Phys. Chem. B 102*, 8201−8208], as well as rotating-frame measurements for both native forms [Banci, L., Bertini, I., Cavazza, C., Felli, I. C., Koulougliotis, D. (1998) *Biochemistry 37*, 12320−12330; Arnesano, F., Banci, L., Bertini, I., Felli, I. C., Koulougliotis, D. (1999) *Eur. J. Biochem*. *260*, 347−354], are already available in the literature. It is found that GdmCl tends to increase the internal mobility, although some residues are rigidified on both time scales. In the milli- to microsecond time scale, the tendency to increased mobility is reflected in a decrease in the τ_{ex} values rather than in the number of residues experiencing conformational equilibria. In the nano- to picosecond time scale, the tendency to increased mobility is indicated by an overall decrease in the S^2 values. Color pictures are reported to visually show these effects. On the fast time scale, the B form is more mobile than the A form, reflecting the different stability with respect to unfolding. The increase in mobility upon addition of denaturant largely occurs around the heme pocket, which facilitates the release of the heme. The relevance of the internal motions with respect to the early steps of the unfolding process is also analyzed and discussed.

The understanding of the factors determining the stability and the biological properties of a protein requires knowledge of the structure and the dynamical properties under a variety of conditions. Within this frame, in the present paper we report a further characterization from the mobility point of view of the soluble fragment of microsomal cytochrome b_5[1] (cyt b_5) from rat in the presence of the denaturant guanidinium chloride (GdmCl).

Cyt b_5 is an amphipathic protein consisting of a hydrophilic (heme-containing) fragment and a hydrophobic (membrane-bound) fragment located in the endoplasmic reticulum of hepatic cells (*1*). It is a ubiquitous protein in many living organisms, and its heme-containing component is involved in a wide variety of biological processes, having the function of shuttling one electron between proteins taking part in the process (*2*−*7*). In addition, this water-soluble domain, constituted by 98 residues, is efficiently expressed in *E. coli* (*1*), retaining fully its activity (*8*), and consequently provides an excellent model system for a variety of biophysical studies. Cyt b_5 contains a *b* type heme moiety. The iron bound to the porphyrin is six-coordinate with two axial histidines (His 39 and His 63) and cycles between 2+ and 3+ oxidation states. As the heme is not covalently attached to the protein but is bound only through the bonds between the iron and the two axial histidines, it can be present in two different orientations, one differing from the other by a 180° rotation around the $\alpha-\gamma$ meso direction. The ratio between the forms, which are called A and B hereafter, depends on the organism, i.e., on the residues present around the heme (*9*−*13*). In the case of the expressed rat microsomal isoenzyme, this ratio (A:B) is approximately 60:40.

The overall folding of the rat protein (*14*) is that typical of cyt b_5 proteins (*15*−*17*). It is constituted by six α-helices and four short β-strands. The heme binding pocket is formed

† This work was supported by the European Community (TMR-LSF Contract ERBFMGECT950033, TMR Contract FMRX-CT98-0218, to L.B.), by Italian CNR (Progetto Finalizzato Biotecnologie 99.00509.PF49), and by MURST-ex 40%. D.K. wishes to thank the TMR Program of the European Union for a postdoctoral fellowship (Contract ERBFMBICT9600994).

* To whom correspondence should be addressed at CERM and Department of Chemistry, University of Florence, Via L. Sacconi, 6, Sesto Fiorentino, Italy. Telephone: +39 055 4209272. Fax: +39 055 4209271. E-mail: bertini@cerm.unifi.it.

‡ Present Address: National Center for Scientific Research (NCSR) DEMOKRITOS, Institute of Materials Science, 15310 Aghia Paraskevi, Athens, Greece.

[1] Abbreviations: GdmCl, guanidinium chloride; cyt b_5, cytochrome b_5; $R_{1\rho}$, rotating-frame relaxation rate; $R_{1\rho}^{OFF}$, off-resonance rotating-frame relaxation rate.

10.1021/bi992756k CCC: $19.00
Published on Web 05/20/2000

by four helices, two above (α4 and α5) and two below (α2 and α3) the heme moiety. The internal side of the pocket, which constitutes the hydrophobic core of the protein, is formed by four β-strands, two parallel (β1 and β2) and two antiparallel (β3 and β4), which form a small β-sheet.

For the rat isoenzyme, the solution structures of both the A and the B forms (*14*, *18*), as well as the solution structure of the A form in the presence of 2 M GdmCl (*19*), are available. Furthermore, the internal motions for the oxidized and the reduced A forms have been characterized, both on the milli- to microsecond (*20*) and on the nano- to picosecond time ranges (*21*, *22*). Finally, the dynamical characterization in the milli- to microsecond time range is available for the oxidized B form (*18*).

Addition of 2 M GdmCl induces a "destabilized" conformation (*23*, *24*), in which some significant structural changes occur around the heme binding pocket (*19*). A key hydrogen bond for the heme binding to the protein, i.e., that between a propionate group and the peptidic NH of Ser 64, is broken upon addition of 2 M GdmCl, and helix α5, which constitutes one side of the heme binding pocket, is shortened. Furthermore, two β-strands (β2 and β3) move apart from each other, thus disrupting the β-sheet. Other structural changes are observed around the heme, involving residues 33−38 (helix α2) and 62−64 (end of helix α4 − beginning of helix α5). On the other hand, most of the secondary structural elements are still present. This destabilized state occurs just before the release of the heme moiety and the formation of a denatured state and thus represents one of the early steps in its unfolding process.

In the present paper, we analyze the dynamical properties, over different time ranges, of both forms of cyt b_5 in the above protein state. Furthermore, we compare such results with those of the two forms of the native protein, which we have completed during this research. Some studies have addressed the structural and dynamical properties of denatured states of proteins (*25*−*28*, *29* and references therein), but they were mainly devoted to systems that are highly unfolded and therefore only partially structured. The role of covalent bonds, such as those of disulfide bridges (*30*−*32*) or those of an Fe_4S_4 cluster bound to cysteine residues (*33*−*35*), has been also addressed, but again the investigated systems had a sizable loss of secondary structure.

This study, following the structural characterization of the cyt b_5 conformation in the presence of 2 M GdmCl (*19*) and the recent published dynamical characterization of the apo form of cyt b_5 (*36*), will give insights into the role of a metal-containing cofactor in determining interactions relevant to the protein stability and folding and into the importance of internal motions over a quite broad range of rates for the events occurring during the early steps of the unfolding process.

MATERIALS AND METHODS

Sample Preparation. Rat microsomal cyt b_5 was isolated as previously described (*1*). An aliquot of GdmCl from a stock solution of 7 M (100 mM phosphate buffer, pH 7.0) was added to an ∼3.5 mM solution of oxidized cyt b_5 to reach 2 M GdmCl final concentration. The sample shows the same NMR spectra as the sample used to determine its three-dimensional structure in solution (*19*). Both the final native and the 2 M GdmCl samples were about 2.7 mM in protein concentration, in 100 mM phosphate buffer at pH 7.0.

NMR Spectroscopy. All NMR experiments were carried out at 298 K, on a Bruker Avance 600 NMR spectrometer operating at a proton Larmor frequency of 600.13 MHz. The ^{15}N off-resonance rotating-frame relaxation rates ($R_{1\rho}^{OFF}$) were measured as a function of the effective magnetic field amplitude (ω_{eff}) by using a pulse sequence previously reported (*37*). The ^{15}N RF irradiation was applied with an amplitude ω_1 and with an offset $\Delta\omega$ with respect to the center of the amide nitrogen resonances, determining an effective magnetic field amplitude ω_{eff} [$\omega_{eff} = (\Delta\omega^2 + \omega_1^2)^{1/2}$], which makes an angle of $\theta = \arctan(\omega_1/\Delta\omega)$ with the y axis. ω_{eff} was changed by changing both the ω_1 amplitude and the carrier frequency. Experiments were performed with four different values of the angle θ (25, 30, 35, and 50°) to increase the range of ω_{eff}. The ω_1 amplitude was increased and decreased gradually in a trapezoidal fashion to achieve adiabatic rotation of the magnetization to the effective magnetic field axis (*38*). During the application of the continuous wave spin-lock field at the ^{15}N frequency, decoupling of the protons was achieved with Waltz-16 pulse decoupling sequence (*39*) to avoid creation of antiphase ^{15}N magnetization via cross-correlation processes (of the type N_xI_z, where N and I are the nuclear spin operators of the ^{15}N and the directly bound ^{1}H nucleus, respectively). The decoupling power was set to 2670 Hz in all experiments. The INEPT transfer delay was set to 5.0 ms, which corresponds to a duration slightly less than 1/[2J(^{1}H−^{15}N)] (*40*). The resulting ω_{eff} values used in the measurements of $R_{1\rho}^{OFF}$ were 1830, 2030, 2270, 2450, 2490, 2710, 3030, 3330, 3660, 4040, 4200, and 4520 Hz. For each ω_1 amplitude value, a series of 2D experiments was performed in which the relaxation delay T was set to the values of 10, 20, 36, 50, 60, 86, 100, 150, 200, 300, and again 10 ms. A further 2D spectrum without the period of spin-lock field was also acquired to measure the initial magnetization. All experiments were recorded with a spectral width of 2130 Hz in the F_1 (^{15}N frequency) dimension and of 8390 Hz in the F_2 (^{1}H frequency) dimension. A total of 160 experiments in t_1, each of 2048 real data points, were recorded. Each free induction decay comprised 16 scans. The measuring time for every 2D spectrum was approximately 1 h. Quadrature detection in F_1 was obtained by using the TPPI method (*41*).

The ^{15}N longitudinal relaxation rates, R_1, were measured as previously described (*42*) by using delays in the pulse sequence of 10, 20, 40, 80, 120, 180, 240, 320, 500, 1000, 1500, and 2000 ms. The ^{15}N transverse relaxation rates, R_2, were measured by using the CPMG sequence as described elsewhere (*42*, *43*). The relaxation delays used were 7.7, 15.4, 30.8, 46.2, 61.6, 77, 100, 154, 231, and 308 ms. The heteronuclear ^{1}H−^{15}N NOEs used the water flip-back method to avoid saturation of the amide resonances (*44*). The acquisition parameters for R_1 and R_2 rates and ^{1}H−^{15}N NOEs were the same as those used for the $R_{1\rho}^{OFF}$ measurement except that a total of 192 experiments were recorded for each 2D spectrum, each comprising eight scans for R_1 and R_2 experiments and 40 scans for ^{1}H−^{15}N NOE experiments.

Sequence-specific assignment of the ^{1}H and ^{15}N resonances of cyt b_5 in the native oxidized state (for both A and B forms) is already available in the literature (*14*, *18*, *45*). The ^{1}H

chemical shifts of the oxidized enzyme in the presence of 2 M GdmCl were recently determined for the A form (*19*) and aided the assignment of the ^{15}N resonances performed in the present work. The ^{1}H and ^{15}N resonances of the B form in the presence of 2 M GdmCl have been assigned in the present paper.

Data Processing. All 2D NMR data were processed on a Silicon Graphics workstation using the UXNMR Bruker software. Only the downfield part of the spectra (in the ^{1}H dimension), containing the H_N-N connectivities (5−12 ppm), was kept for the data analysis. All spectra were transformed with 4 × 1K points in the F_2 and F_1 dimensions, respectively. All spectra acquired with the same ω_1 amplitude were processed by using the same processing parameters (phasing parameters, baseline correction, etc.). Subsequent integration of cross-peaks for all spectra was performed by using the standard routine of the UXNMR program.

Determination of Relaxation Rates. Relaxation rates R_1, $R_{1\rho}^{OFF}$, and R_2 were determined by fitting the cross-peak intensities (I) measured as a function of the delay (T) within the pulse sequence, to a single-exponential decay by using the Levenburg-Marquardt algorithm (*46*, *47*) according to the following equation:

$$I(T) = A + B\exp(-RT) \quad (1)$$

where A, B, and R were adjustable fitting parameters. A program that uses a Monte Carlo approach to estimate the error on the rates (*37*, *48*, *49*) was used for this purpose. For $R_{1\rho}^{OFF}$ and R_2, the phase cycle was chosen so that the magnetization relaxes to zero for long relaxation delays. Thus, in these two cases, A was set equal to zero in the fitting procedure. The error bars for $R_{1\rho}^{OFF}$ correspond to the experimental error averaged over all the applied spin-lock powers. The error value for $R_{1\rho}^{OFF,cor}$ (see later) includes the errors in the measurement of both $R_{1\rho}^{OFF}$ and R_1. The error bars for R_2 correspond to the experimental error averaged over two measurements.

Analysis of the Rotating Frame Relaxation Rates. The off-resonance relaxation rate $R_{1\rho}^{OFF}$ of a ^{15}N spin participating in a conformational exchange process is given by (*50*−*53*):

$$R_{1\rho}^{OFF} = R_1\cos^2\theta + R_{1\rho}^{ON,\infty}\sin^2\theta + K\sin^2\theta\,\frac{\tau_{ex}}{1+\tau_{ex}^2\omega_{eff}^2} \quad (2)$$

where R_1 is the longitudinal relaxation rate, $R_{1\rho}^{ON,\infty}$ is the on-resonance rotating-frame relaxation rate with an infinitely large effective field amplitude, and τ_{ex} is the correlation time for the exchange process involving the spin under observation. K is a constant equal to $p_a p_b \delta\Omega^2$, where p_a and p_b are the relative populations of the two states a and b between which the exchange process occurs and $\delta\Omega$ is chemical shift difference of the resonating nucleus between these two states. Equation 2 is valid when $\delta\Omega\tau_{ex} \ll 1$ and off-resonance effects are neglected. However, this equation can be used even when the two conditions are violated (*30*).

As explained elsewhere (*20*, *37*), for $R_{1\rho}$ values measured with different ω_{eff}, the angle θ_i is not strictly constant for all spins, and therefore the $R_{1\rho}$ values should be corrected as follows:

$$\frac{R_{1\rho}^{OFF} - R_1\cos^2\theta}{\sin^2\theta} = R_{1\rho}^{ON,\infty} + K\frac{\tau_{ex}}{1+\tau_{ex}^2\omega_{eff}^2} = R_{1\rho}^{OFF,cor} \quad (3)$$

Equations 2 and 3 indicate that, in the presence of exchange equilibria, the values of $R_{1\rho}^{OFF}$ and $R_{1\rho}^{OFF,cor}$ depend on the applied ω_{eff}. By fitting the experimental $R_{1\rho}^{OFF,cor}$ values to eq 3, the correlation time τ_{ex} for the exchange process can be estimated. The fits were performed by using the nonlinear fitting routine based on the Levenberg−Marquardt algorithm (*46*, *47*) as described in the literature (*48*). K, τ_{ex}, and $R_{1\rho}^{ON,\infty}$ are adjustable parameters, and the experimental value of R_2 can be used as an additional data point, as it equals the $R_{1\rho}^{OFF,cor}$ limit at $\omega_{eff} = 0$. If no exchange process is present (i.e., $\tau_{ex} = 0$), $R_{1\rho}^{OFF,cor}$ is independent of ω_{eff} and equal to $R_{1\rho}^{ON,\infty}$. The accessible range for the exchange processes to be detected, with the present available ω_{eff} values, varies approximately between 30 and 250 μs. Therefore, exchange processes could be, even if present, either "too fast" ($\tau_{ex} <$ 30 μs) or "too slow" ($\tau_{ex} >$ 250 μs) to be detected from the dependence of $R_{1\rho}^{OFF,cor}$ on ω_{eff}. In the case of a fast process (i.e., faster than the lower limit of τ_{ex}), $R_{1\rho}^{OFF,cor}$ appears constant with ω_{eff} but larger than the average $R_{1\rho}^{OFF,cor}$ values observed for the other nuclei not participating at any exchange process and equal to $R_{1\rho}^{ON,\infty} + K\tau_{ex}$. In the case of a slow process (i.e., lower than the upper limit of τ_{ex}), $R_{1\rho}^{OFF,cor}$ appears to be independent of ω_{eff} and equal to $R_{1\rho}^{ON,\infty}$. Thus, such slow processes cannot be identified through $R_{1\rho}^{OFF}$ alone. However, in the limit of $\omega_{eff} = 0$, $R_{1\rho}^{OFF,cor} = R_{1\rho}^{ON,\infty} + K\tau_{ex} = R_2$. Thus, by independently measuring R_2, it is possible to identify these slow processes.

Analysis of Longitudinal and Transverse Relaxation and of Heteronuclear NOEs with the Model-Free Approach. The experimental longitudinal and transverse relaxation rates and the heteronuclear NOEs have been analyzed with the Model-Free 4.0 program (*54*), within the Lipari−Szabo approach (*55*). This program models overall rotational diffusion using an axially symmetric diffusion tensor **D**. R_1, R_2, and NOE values for ^{15}N spins are determined by the dipolar coupling with the attached proton and, for R_1 and R_2, also by the chemical shift anisotropy of the nitrogen spins. The equations for these rates, in terms of spectral density functions $J(\omega)$, are reported in the literature (*56*). R_2 can also contain a contribution originating from exchange, R_{ex}. In the present work, we have used an independent experimental method (^{15}N rotating-frame relaxation) to specifically probe and accurately determine the exchange processes (R_{ex}). This allows us to safely restrict the analysis of R_1, R_2, and NOEs for the estimation of the values of the order parameter and the correlation time for the internal motions.

Within the Model-Free approach (*48*, *54*), the spectral density functions $J(\omega)$ can be expressed as a function of the overall rotational correlation time τ_m, of the order parameter S^2, and of the correlation time for internal motions, which can be considered as arising from two components, one describing faster (τ_f) and one slower (τ_s) motions (collectively called τ_e) but always faster than τ_m.

Initially, the best fitting is made by using the following equation (*57*) for the spectral densities in the approximation of isotropic tumbling:

$$J(\omega) = \frac{2}{5}\left[\frac{S^2\tau_m}{1 + (\omega\tau_m)^2}\right] \quad (4)$$

where the only variable parameter is S^2. For those HN vectors, whose internal motions are librations with a small amplitude occurring with a very fast correlation time (τ_f < 10 ps), it can be assumed that the dominating contribution to the spectral density is given by the overall reorientation of the molecule, modulated by τ_m, with the value of S^2 accounting for the reduction of relaxation rates of the HN vector due to the very fast internal librations. This is referred to as model 1 in the literature (*48*).

When the fitting using eq 4 is poor, a second term is added to the spectral density function, according to the following equation:

$$J(\omega) = \frac{2}{5}\left[\frac{S^2\tau_m}{1 + (\omega\tau_m)^2} + \frac{(1 - S^2)\tau_f'}{1 + (\omega\tau_f')^2}\right] \quad (5)$$

where $\tau_f'^{-1} = \tau_m^{-1} + \tau_f^{-1}$, and τ_f is the effective correlation time for internal motions on a faster time scale than τ_m (τ_f < 200 ps). Within this motional model, the correlation time for the intramolecular motions of the HN vector is used as a further parameter in the fitting and an F-statistic test (*54*) has been applied to check that the improvement in the fitting is just not due to the introduction of a new parameter but to a physical requirement. Note that the sum of the scalar factors containing S^2 in eq 5 is normalized and that the quantity that multiplies the second member in square brackets of eq 5 is the complement to unity of S^2. This is referred to as model 2 in the literature.

In some cases, a contribution to R_2 due to exchange processes (R_{ex}) can be operative and is included as a fitted parameter in the calculations. When this term is operative, models 1 and 2 are called models 3 and 4 in the literature, respectively.

When the above motional models were not fitting the experimental data, the spectral density function is described by the following equation:

$$J(\omega) = \frac{2}{5}\left[\frac{S^2\tau_m}{1 + (\omega\tau_m)^2} + \frac{(S_f^{\,2} - S^2)\tau_s'}{1 + (\omega\tau_s')^2}\right] \quad (6)$$

where $\tau_s'^{-1} = \tau_m^{-1} + \tau_s^{-1}$ and τ_s is the effective correlation time for internal motions on a slow time scale but still faster than τ_m (200 ps < τ_s < τ_m), $S^2 = S_f^{\,2} \times S_s^2$ is the square of the generalized order parameter characterizing the amplitude of the internal motions, and $S_f^{\,2}$ and S_s^2 are the squares of the order parameters for the internal motions on the fast and slow time scales, respectively. Within this model, very fast librations (characterized by a correlation time τ_f < 10 ps) are described by $S_f^{\,2}$ that contributes to reduce the generalized order parameter, and motions on a slower time scale are accounted for introducing a correlation time τ_s as variable parameter in the fitting. This is referred to as model 5 in the literature. This model is used to fit relaxation data for HN vectors experiencing more complex internal motions, typical of partially or completely unfolded proteins, where the increased overall mobility is associated with the presence of collective motions.

The effect of the anisotropy of molecular reorientation on the Model-Free analysis has been recently investigated (*58*−*60*). If ignored, it can produce erroneous results on the identification of conformational exchange processes even for quite modest anisotropies ($D_{||}/D_\perp = 1.3$, where $D_{||}$ and $D_\perp$ are the parallel and perpendicular components, respectively, of an axially symmetric diffusion tensor) (*59*). On the contrary, even in the presence of relatively large anisotropic motions ($D_{||}/D_\perp = 2.0$), the S^2 values are minimally affected (less than 6% and in most cases less than 3%)(*58*). In the present analysis, we have used an axially symmetric model to account for the global rotational motion. In such a condition, depending on the selected motional model for the specific HN vector, the spectral densities are given by eqs 4−6, where the quantities in square brackets become the argument of the summation over three components of the diffusion tensor **D**, and τ_m^{-1} assumes the following values: $\tau_{m1}^{\ -1} = 6D_\perp$, $\tau_{m2}^{\ -1} = 5D_\perp + D_{||}$, $\tau_{m3}^{\ -1} = 2D_\perp + 4D_{||}$. The three terms of the summation are multiplied by $A_1 = (3\cos^2\theta - 1)^2/4$, $A_2 = 3\sin^2\theta\cos^2\theta$, and $A_3 = (3/4)\sin^4\theta$, respectively, and θ is the angle between the N−H bond vector and the unique axis of the principal frame of the diffusion tensor (*61*−*63*).

Having available the three-dimensional structures of cyt b_5 in the native state (for A and B forms) and in 2 M GdmCl (only for A form, while the B form is assumed to have a similar structure), then the rotational diffusion tensor can be estimated from the R_2/R_1 ratio. Once the best model for the molecular motions is selected, the overall τ_m, the ratio $D_{||}/D_\perp$, and the internal motional parameters for each spin are optimized by fitting the experimental relaxation parameters R_1, R_2, and NOE to their equations (*56*). Powell minimization algorithm [see W. H. Press et al. (1992) *Numerical Recipes in C*, 2nd ed., section 10.5, Cambridge University Press, New York] has been used.

Dealing with paramagnetic molecules, we should also estimate the possible contribution to the relaxation rates arising from the coupling between the resonating nuclei and the unpaired electrons. While the effect can be sizable on the proton relaxation rates, it is dramatically reduced on the nitrogens, due to their low gyromagnetic ratio. It has been already estimated that the effect could be operative for nitrogens closer than 7 Å to the metal (*64*). In the case of the native form of cyt b_5 (*20*), it has been found that the backbone nitrogen nuclei closest to the heme Fe(III) and involved in exchange processes are within 7.4 and 7.8 Å from the iron. For these nuclei, the paramagnetic contribution to the ^{15}N longitudinal relaxation rate was estimated to be in the range of 0.02−0.05 Hz (*20*), which is very small with respect to the experimentally observed values.

RESULTS

The backbone dynamics of oxidized rat microsomal cyt b_5 in the presence of 2 M GdmCl was investigated at different time scales, i.e., in the milli- to microsecond and in the nano- to picosecond time scales. As already discussed in the introduction, the protein is present in two forms (A and B) containing the heme group rotated by 180°, one with respect to the other around the $\alpha-\gamma$ meso direction. The dynamical properties have been subsequently compared with those of the two forms in the native state.

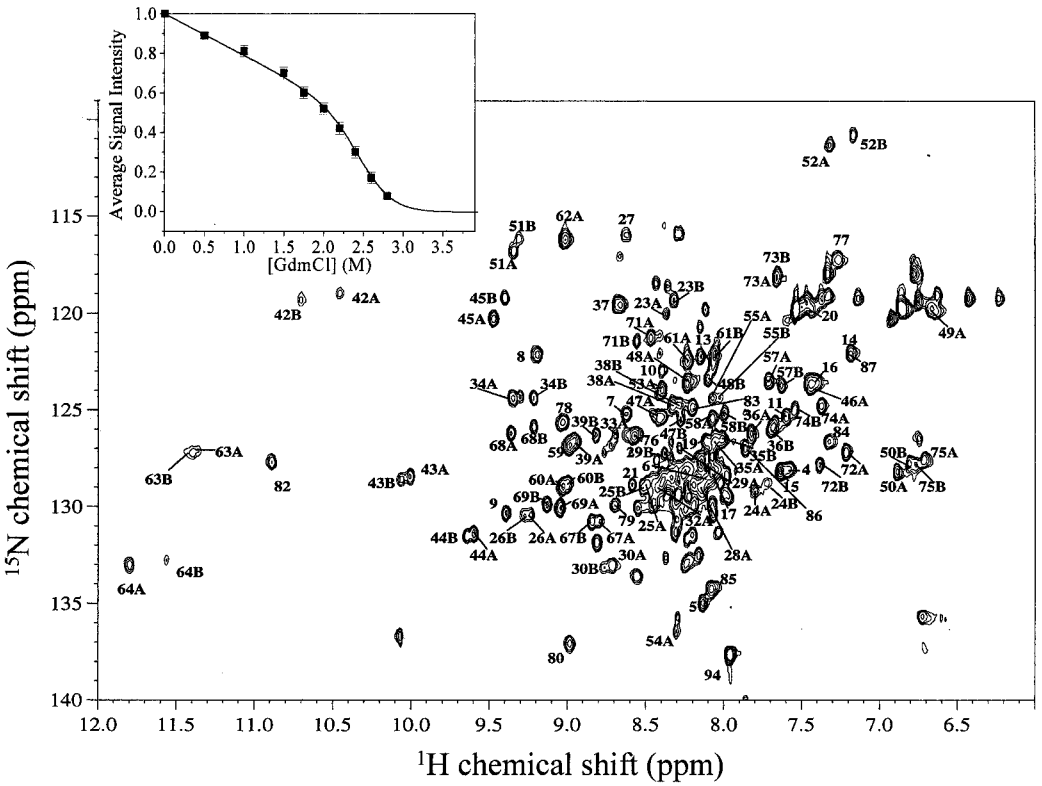

FIGURE 1: ^{1}H−^{15}N HSQC 600-MHz spectrum of oxidized rat microsomal cyt b_5 in 2 M GdmCl (100 mM phosphate buffer, pH 7, at 298 K). Peaks of both A and B forms are labeled according to the residue assignment. The inset reports the change in average signal intensity of the paramagnetically shifted resonances of the B form of oxidized rat microsomal cyt b_5 as a function of GdmCl concentration. The solid curve represents a fit of the normalized experimental intensities to eq 7.

^{1}H and ^{15}N resonance assignments, as well as the solution structures, are available in the literature for both oxidized forms (*14*, *18*) and for the oxidized A form in the presence of 2 M GdmCl (*19*). The assignment of the ^{1}H and ^{15}N backbone NH resonances of the oxidized B form of cyt b_5 in the presence of 2 M GdmCl was performed in the present study (see Figure 1).

The spectroscopic parameters for the nano- to picosecond time scale without denaturant were also available in the literature (*21*), but we remeasured them to make more meaningful the comparison with the species in the presence of denaturant. The present data substantially agree with the literature ones.

NMR Titration with GdmCl. Upon addition of GdmCl up to ~1.8 M concentration, the paramagnetically shifted signals show some change in the shifts and a small decrease in intensity, thus indicating only small structural changes. When the concentration of denaturant is increased, the intensity of these signals rapidly decreases and becomes essentially zero at a concentration of about 3.0 M. This indicates that the heme is released from the protein by the addition of GdmCl. The 1D ^{1}H NMR spectrum as well as the ^{15}N−^{1}H HSQC map of the protein at 3 M GdmCl are very close to that observed for a random coil state. The behavior with GdmCl suggests the presence of slow exchange between the species minimally perturbed or native (N) and the denatured form (U). The changes in intensity of the paramagnetically shifted signals as a function of GdmCl concentration are reported as the inset in Figure 1 and have been fitted, as already described for the A form (*19*), to a two-state N ↔ U model for both A and B forms, according to the following relation (*65*−*67*):

$$y_{obs} = \{y_N + \alpha_N[\text{GdmCl}] + y_U + \alpha_U[\text{GdmCl}] \exp[(-\Delta G^\circ + m[\text{GdmCl}])/RT]\}/\{1 + \exp[(-\Delta G^\circ + m[\text{GdmCl}])/RT]\} \quad (7)$$

where y_{obs} is the normalized signal intensity; $R = 8.3$ J K^{-1} mol^{-1}; y_N, y_U, and α_N, α_U represent intercepts and slopes of the native (N) and unfolded (U) baselines, respectively; and m is a parameter reflecting the steepness of the unfolding transition. This analysis provides ΔG°, that represents the free energy of the unfolding process in the absence of denaturant, and m, a parameter reflecting the steepness of the unfolding transition. From the least-squares fit, we obtain $\Delta G^\circ = 29 \pm 3$ kJ mol^{-1} and $m = 11 \pm 1$ kJ mol^{-1} M^{-1}, for the A form of the protein, and $\Delta G^\circ = 22 \pm 3$ kJ mol^{-1} and $m = 9 \pm 1$ kJ mol^{-1} M^{-1} for the B form. These values indicate that the B form, as already observed (*18*, *22*, *68*), is slightly less stable with respect to the unfolding process than the A form. Values available in the literature (*24*) obtained through fluorescence measurements report ΔG° of 26.5 kJ mol^{-1} and $m = 8.6$ kJ mol^{-1} M^{-1} for the bovine isoenzyme that contains essentially only the A form.

Relaxation Properties of Oxidized cyt b_5 in the Presence of 2 M GdmCl. (1) Rotating Frame Experiments. The off-resonance rotating-frame relaxation rates $R_{1\rho}^{OFF}$ and the transverse relaxation rates R_2 of the backbone amide nitrogens of oxidized cyt b_5 in the presence of 2 M GdmCl (Figure 1 of the Supporting Information) were measured for those ^{15}N resonances that do not show overlap and therefore can be accurately integrated. They correspond to 66 ^{15}N nuclei, as several could not be detected due to proton exchange and 22 were unresolved. Out of these 66 ^{15}N resonances, 40 were individually resolved for the A and B species. The depen-

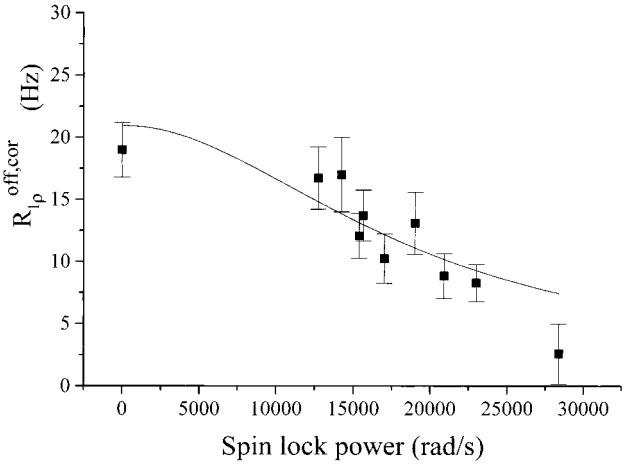

FIGURE 2: Off-resonance rotating-frame relaxation rates, $R_{1\rho}^{OFF,cor}$, of the backbone nitrogen of Thr 33 as a function of the effective magnetic field amplitude, ω_{eff}, for the A form of oxidized rat microsomal cyt b_5 in the presence of 2 M GdmCl. The solid curve represents the fit to a Lorentzian-type function (eq 3).

dence of their $R_{1\rho}^{OFF,cor}$ values with ω_{eff} was examined. Ten ^{15}N for the A form and 12 ^{15}N for the B form display a dependence of $R_{1\rho}^{OFF,cor}$ with ω_{eff}. Six more ^{15}N resonances, which are degenerate for the two forms, also show a dependence of the $R_{1\rho}^{OFF,cor}$ on ω_{eff}.

As discussed in Materials and Methods, an increase of $R_{1\rho}^{OFF,cor}$ with decreasing ω_{eff} is indicative of the presence of exchange processes in the milli- to microsecond time scale. The correlation times for the exchange processes, τ_{ex}, can be obtained by fitting the data to eq 3. An example of $R_{1\rho}^{OFF,cor}$ dependence on ω_{eff} and of its fitting to eq 3 is shown in Figure 2. As discussed before (*20*), the paramagnetic contribution to the nitrogen relaxation rates is negligible, due to the low gyromagnetic ratio of the ^{15}N nucleus. The values estimated for τ_{ex} range between ~35 μs (for Ala67 in the B form) and ~85 μs (for Ser 64 in the A form) and are reported in Table 1. The secondary structural elements of the protein to which these residues belong are reported as well.

The six degenerate signals belonging to residues 19, 27, 59, 78, 80, and 85, which also experience conformational equilibria, provide a τ_{ex} that is an average between those for the two species. Since the shifts are the same, it is reasonable to assume that the mobility for the two species is similar, even if this reasoning cannot be proved. The exchange correlation time for the process has been determined for 16 residues (including the degenerate ones) for the A form and 18 for the B form. A pictorial representation of these results is shown in Figure 3 for the A form (panel a) and for the B form (panel c).

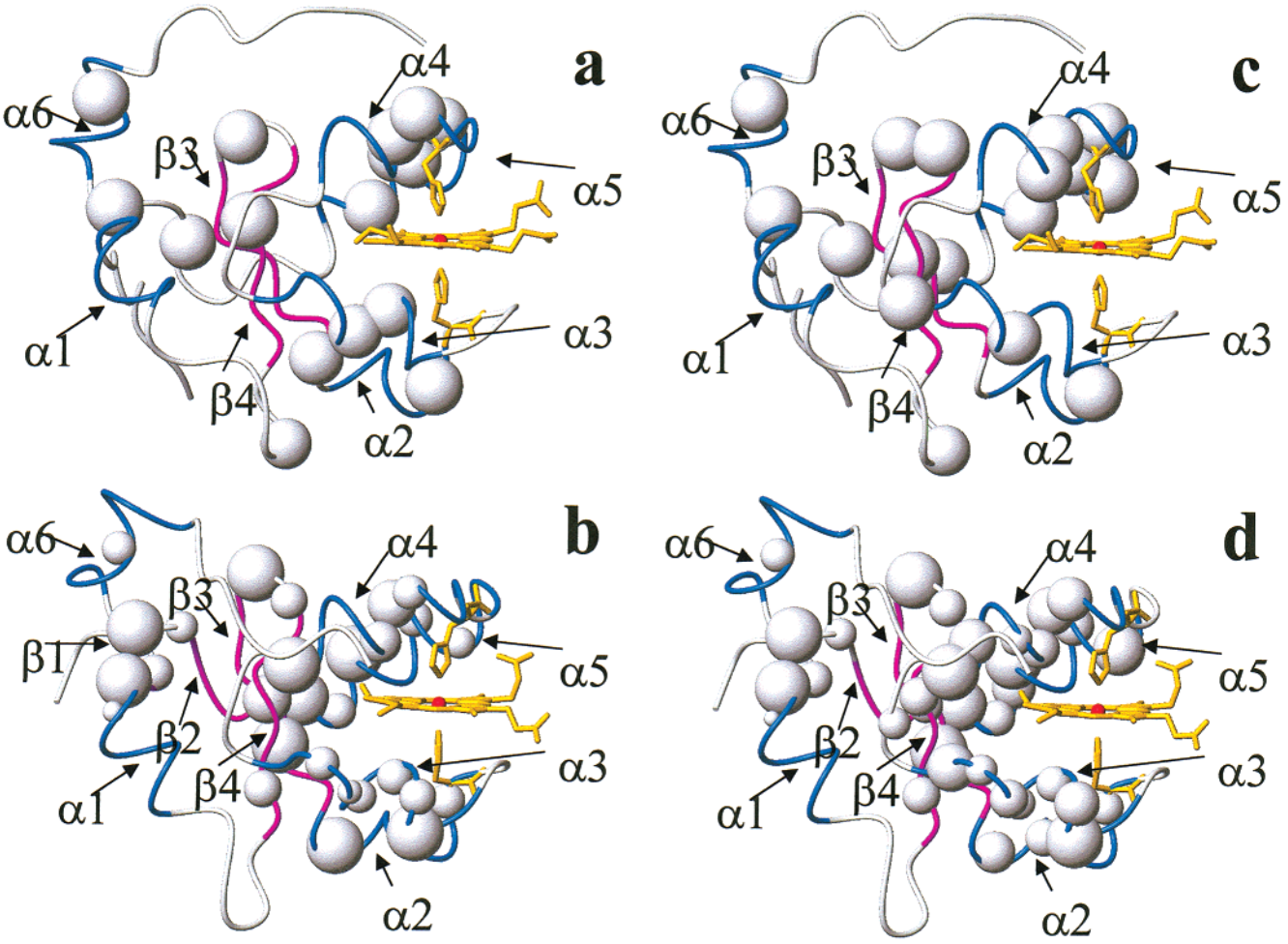

FIGURE 3: Mapping of ^{15}N exchange rates in the protein frame of the A form of cyt b_5 in 2 M GdmCl (a) and in the native state (b) and of the B form of cyt b_5 in 2 M GdmCl (c) and in the native state (d). Amide backbone nitrogens participating in conformational exchange processes in the milli- to microsecond time scale are represented as spheres whose radius is proportional to τ_{ex}^{-1}. Secondary structure elements are indicated: α-helices in blue and β-strands in magenta.

Table 1: Exchange Correlation Times (τ_{ex}) Estimated for the Amide Backbone Nitrogens of Oxidized cyt b_5 (A and B forms) in the Native State and in the Presence of Denaturant (2 M GdmCl)[a]

	2 M GdmCl			native form		
residue[b]	secondary[c] element	cyt b_5 B[d,e] $\tau_{ex}(\mu s)$	cyt b_5 B[d,e] $\tau_{ex}(\mu s)$	secondary element	cyt b_5 A[d,e] $\tau_{ex}(\mu s)$	cyt b_5 B[d,e] $\tau_{ex}(\mu s)$
*Lys 5	***	■	■	β1	160 ± 45	160 ± 45
*Leu 9	α1	■	■	α1	50 ± 25	50 ± 25
*Glu 10	α1	■	■	α1	250 ± 55	250 ± 55
*Lys 19	loop	80 ± 25	80 ± 25	loop	■	■
Trp 22	β4	▼	▼	β4	155 ± 30	155 ± 30
Ile 24	β4	40 ± 10	■	β4	■	145 ± 50
His 26	turn	■	40 ± 5	turn	160 ± 40	155 ± 60
*His 27	turn	60 ± 15	60 ± 15	turn	<40	<40
Tyr 30	β3	■	50 ± 10	β3	90 ± 30	175 ± 65
Asp 31	β3	▼	▼	β3	<40	<40
Thr 33	***	60 ± 10	■	α2	■	■
Lys 34	α2	■	■	α2	<40	130 ± 50
Leu 36	α2	■	■	α2	■	155 ± 70
Glu 38	α2	40 ± 5	40 ± 5	α2	▼	▼
His 39	***	■	■	α2	165 ± 45	175 ± 80
Glu 44	α3	■	■	α3	<40	<40
Val 45	α3	■	■	α3	160 ± 45	110 ± 35
Leu 46	α3	60 ± 10	■	α3	165 ± 50	165 ± 50
Arg 47	α3	60 ± 10	60 ± 10	α3	180 ± 45	185 ± 50
Glu 48	α3	■	■	α3	230 ± 60	150 ± 75
Gln 49	α3	▼	▼	α3	175 ± 35	190 ± 90
Ala 50	α3	■	■	α3	■	90 ± 40
Gly 51	turn	■	45 ± 5	turn	■	■
Gly 52	turn	■	■	turn	■	185 ± 65
Ala 54	***	■	■	α4	<40	<40
Thr 55	α4	■	■	α4	■	100 ± 55
Asn 57	α4	■	■	α4	■	190 ± 65
Phe 58	α4	■	50 ± 10	α4	130 ± 35	140 ± 45
*Glu 59	α4	40 ± 10	40 ± 10	α4	90 ± 30	90 ± 30
Asp 60	α4	50 ± 15	■	α4	170 ± 50	110 ± 50
Ser 64	α5	85 ± 15	70 ± 10	α5	■	■
Ala 67	α5	■	35 ± 5	α5	190 ± 55	70 ± 45
Arg 68	α5	60 ± 15	55 ± 15	α5	■	■
Glu 69	α5	50 ± 15	50 ± 10	α5	165 ± 35	140 ± 55
Ser 71	α5	50 ± 10	50 ± 10	α5	■	■
Lys 72	α5	■	■	α5	<40	<40
Thr 73	***	■	■	α5	■	120 ± 65
Tyr 74	***	■	■	α5	165 ± 35	165 ± 65
Ile 75	***	■	50 ± 5	β2	55 ± 25	70 ± 40
*Glu 78	***	50± 15	50± 15	β2	■	■
*Leu 79	***	■	■	turn	185 ± 65	185 ± 65
*His 80	***	40 ± 15	40 ± 15	turn	<40	<40
*Arg 84	α6	■	■	α6	175 ± 55	175 ± 55
*Ser 85	α6	45 ± 10	45 ± 10	α6	■	■

[a] Secondary structural elements to which each amide belongs are also reported. [b] Single asterisk (*) denotes residues with degenerate resonances for both species. [c] Three asterisks (***) denote these residues do not belong anymore to a secondary structural element in 2 M GdmCl. [d] (▼) Resonance not observed. [e] (■) Residues not involved in conformational exchange processes.

(2) Pico- to Nanosecond Mobility. The experimental R_1 and the $^1H-^{15}N$ NOEs are reported in the Supporting Information for both the A and B forms of oxidized cyt b_5 in 2 M GdmCl. By using the Model-Free 4.0 program (*54*), the parameters characterizing the overall and internal mobility within the Lipari-Szabo model (*55*) have been determined for each backbone NH whose signal can be resolved in the 2D maps.

The inertia tensors for each structure have been calculated from the available structures (*14*, *18*, *19*). Initially, the local rotational correlation time values, τ_{mi}, for each **i** amide vector were calculated from the R_2/R_1 ratios (by using those R_2 values that are not affected by exchange processes) and used as input in the evaluation of the axially symmetric diffusion tensor **D** (*69*). The overall correlation time for molecular tumbling, τ_m, and the $D_{||}/D_{\perp}$ ratio were fitted during the last stage of Model-Free calculations after the motional model selections, obtained with the calculated diffusion tensor anisotropy. The $D_{||}/D_{\perp}$ ratio was found to be in the range of 1.2−1.4 for both native and 2 M GdmCl cyt b_5. The overall τ_m values are 7.6 ns and 7.8 ns in 2 M GdmCl for A and B forms, respectively, and 5.6 ns and 5.9 ns in the native protein. The higher τ_m values for the destabilized protein are consistent with an increased viscosity of the solution after addition of denaturant. Meaningful values (i.e., larger than their errors) for the correlation time for fast internal motions, τ_e, were found for 20 residues in both the A and B forms in addition to seven degenerate residues for which average values are obtained (see Table 2). The generalized order parameters S^2 for each residue are reported in Figure 4. Self-consistent results were obtained for 35 backbone NH vectors unique for the A form and 28 for the B form, together with 22 average values for degenerate resonances.

Figure 4 shows that S^2 experiences some scattering along the protein sequence. In addition to residue 94 ($S^2 = 0.44$), which is expected to have a low value for S^2 as is close to

Table 2: Generalized Order Parameters, S^2, and Effective Internal Correlation Times, τ_e (where determined), for the Amide Backbone Nitrogens of Oxidized cyt b_5 (A and B forms) in the Native State and in the Presence of Denaturant

	2 M GdmCl				native			
	A form[b]		B form[b]		A form[b]		B form[b]	
residue[a]	S^{2c}	τ_e[d] (ps)	S^{2c}	τ_e[d] (ps)	S^{2c}	τ_e[d] (ps)	S^{2c}	τ_e[d] (ps)
*Lys 5	0.40 ± 0.10	1800 ± 500[e]	0.40 ± 0.10	1800 ± 500[e]	0.76 ± 0.05	40 ± 20[f]	0.76 ± 0.05	40 ± 20[f]
*Tyr 6	0.37 ± 0.11	2440 ± 700[e]	0.37 ± 0.11	2440 ± 700[e]	▼		▼	
*Tyr 7	0.79 ± 0.06	*g*	0.79 ± 0.06	*g*	0.84 ± 0.04		0.84 ± 0.04	
*Thr 8	0.70 ± 0.05	*g*	0.70 ± 0.05	*g*	0.80 ± 0.04		0.80 ± 0.04	
*Leu 9	0.80 ± 0.06	*g*	0.80 ± 0.06	*g*	0.80 ± 0.05	50 ± 20[f]	0.80 ± 0.05	50 ± 20[f]
*Glu 10	●		●		0.91 ± 0.05	*g*	0.91 ± 0.05	*g*
*Glu 11	▼		▼		0.83 ± 0.04		0.83 ± 0.04	
*Ile 12	▼		▼		0.90 ± 0.04		0.90 ± 0.04	
*Gln 13	0.93 ± 0.05	250 ± 200[e]	0.93 ± 0.05	250 ± 200[e]	0.84 ± 0.05		0.84 ± 0.05	
*Lys 14	▼		▼		0.67 ± 0.09	1000 ± 300[e]	0.67 ± 0.09	1000 ± 300[e]
*His 15	0.74 ± 0.06	*g*	0.74 ± 0.06	*g*	0.84 ± 0.04		0.84 ± 0.04	
*Lys 16	0.93 ± 0.05		0.93 ± 0.05		0.84 ± 0.04		0.84 ± 0.04	
*Asp 17	0.84 ± 0.06	50 ± 30[h]	0.84 ± 0.06	50 ± 30[h]	▼		▼	
*Lys 19	0.70 ± 0.05	30 ± 12[f]	0.70 ± 0.05	30 ± 12[f]	●		●	
*Ser 20	▼		▼		0.91 ± 0.05	*g*	0.91 ± 0.05	*g*
*Thr 21	1.00 ± 0.05		1.00 ± 0.05		0.83 ± 0.05	*g*	0.83 ± 0.05	*g*
Trp 22	▼		▼		1.00 ± 0.05		▼	
Val 23	●		0.91 ± 0.06	71 ± 66[f]	0.85 ± 0.05	70 ± 30[h]	0.90 ± 0.05	*g*
Ile 24	0.85 ± 0.09	150 ± 140[f]	0.65 ± 0.09	16 ± 5[f]	0.88 ± 0.04		0.87 ± 0.05	*g*
Leu 25	0.76 ± 0.05		0.47 ± 0.09	2260 ± 920[e]	0.81 ± 0.04	45 ± 20[h]	0.77 ± 0.04	100 ± 30[h]
His 26	●		0.89 ± 0.05	66 ± 44[f]	0.87 ± 0.05	80 ± 50[f]	0.86 ± 0.05	60 ± 40[f]
*His 27	0.99 ± 0.06	*g*	0.99 ± 0.06	*g*	0.94 ± 0.05	*g*	0.94 ± 0.05	*g*
Lys 28	0.78 ± 0.05		●		0.82 ± 0.04		▼	
Val 29	0.72 ± 0.05	20 ± 10[h]	0.42 ± 0.09	1900 ± 400[e]	0.85 ± 0.04		▼	
Tyr 30	0.76 ± 0.06	*g*	0.49 ± 0.06	11 ± 4[f]	●		0.94 ± 0.05	*g*
Asp 31	▼		▼		0.88 ± 0.05	*g*	0.90 ± 0.05	*g*
Thr 33	0.74 ± 0.06	*g*	●		●		●	
Lys 34	0.80 ± 0.05		0.77 ± 0.04		0.88 ± 0.05		0.97 ± 0.07	*g*
Phe 35	0.78 ± 0.05	15 ± 12[h]	●		0.86 ± 0.05		▼	
Leu 36	0.77 ± 0.05	21 ± 13[h]	0.68 ± 0.08	2200 ± 970[e]	0.80 ± 0.04	45 ± 20[h]	0.82 ± 0.04	160 ± 81[f]
*Glu 37	0.72 ± 0.06	18 ± 10[f]	0.72 ± 0.06	18 ± 10[h]	0.79 ± 0.04		0.79 ± 0.04	
Glu 38	0.81 ± 0.05	25 ± 16[f]	0.79 ± 0.05	21 ± 14[f]	▼		▼	
His 39	0.88 ± 0.05	43 ± 33[h]	0.82 ± 0.04	61 ± 25[h]	0.85 ± 0.05	*g*	0.86 ± 0.05	92 ± 50[f]
Gly 42	0.63 ± 0.05	2200 ± 500[e]	0.55 ± 0.06	17 ± 6[f]	0.75 ± 0.06	900 ± 500[e]	0.76 ± 0.10	1100 ± 825[e]
Glu 43	0.81 ± 0.05		0.89 ± 0.07		▼		▼	
Glu 44	●		●		0.94 ± 0.05	150 ± 150[f]	1.00 ± 0.05	
Val 45	●		●		0.91 ± 0.04		0.78 ± 0.11	*g*
Leu 46	0.77 ± 0.05	*g*	●		0.88 ± 0.05	100 ± 60[f]	●	
Arg 47	0.83 ± 0.05	30 ± 18[f]	0.99 ± 0.05	*g*	0.80 ± 0.05	50 ± 20[f]	0.89 ± 0.05	100 ± 70[f]
Glu 48	0.85 ± 0.06	40 ± 25[h]	0.87 ± 0.05	60 ± 30[h]	0.87 ± 0.05	65 ± 40[f]	0.87 ± 0.05	87 ± 51[f]
Gln 49	▼		▼		0.91 ± 0.04		0.80 ± 0.06	100 ± 56[f]
Ala 50	0.75 ± 0.06	14 ± 10[f]	0.65 ± 0.05	16 ± 4[f]	0.89 ± 0.05		0.87 ± 0.05	50 ± 35[f]
Gly 51	0.72 ± 0.10	2050 ± 1170[e]	●		●		0.83 ± 0.07	
Gly 52	0.83 ± 0.05	50 ± 25[h]	0.79 ± 0.05	38 ± 17[h]	●		▼	
Asp 53	0.77 ± 0.05	21 ± 13[h]	●		▼		▼	
Ala 54	0.59 ± 0.04	20 ± 6[h]	●		0.74 ± 0.05	20 ± 10[f]	0.81 ± 0.05	20 ± 18[f]
Thr 55	0.85 ± 0.05	*g*	1.00 ± 0.05		●		0.50 ± 0.11	2000 ± 300[f]
Asn 57	0.84 ± 0.05	33 ± 22[h]	0.76 ± 0.05	27 ± 12[f]	0.90 ± 0.04	110 ± 80[h]	0.99 ± 0.05	
Phe 58	●		●		0.86 ± 0.03	230 ± 200[f]	0.92 ± 0.07	
*Glu 59	0.99 ± 0.05	*g*	0.99 ± 0.05	*g*	0.94 ± 0.05	*g*	0.94 ± 0.05	*g*
Asp 60	0.75 ± 0.06	23 ± 13[f]	0.93 ± 0.05		0.85 ± 0.05	32 ± 26[f]	0.91 ± 0.10	200 ± 150[f]
Val 61	0.84 ± 0.05		0.89 ± 0.05	39 ± 33[h]	0.83 ± 0.04		0.84 ± 0.06	
Gly 62	0.80 ± 0.05	18 ± 14[h]	●		0.87 ± 0.04		0.87 ± 0.05	
Ser 64	0.99 ± 0.05		0.41 ± 0.12	10 ± 5[f]	0.91 ± 0.04		0.84 ± 0.04	85 ± 40[h]
Ala 67	1.00 ± 0.05		0.78 ± 0.05	*g*	0.88 ± 0.05	85 ± 55[f]	0.88 ± 0.05	
Arg 68	0.76 ± 0.06	24 ± 14[f]	1.00 ± 0.05	*g*	0.79 ± 0.04	50 ± 20[h]	0.78 ± 0.06	
Glu 69	1.00 ± 0.05	*g*	0.91 ± 0.04	40 ± 39[f]	0.87 ± 0.05	*g*	0.89 ± 0.05	115 ± 80[f]
Ser 71	0.87 ± 0.05	*g*	0.76 ± 0.05	32 ± 14[f]	0.86 ± 0.04		0.84 ± 0.05	55 ± 30[h]
Lys 72	0.80 ± 0.06	*g*	0.60 ± 0.09	3000 ± 1300[e]	0.87 ± 0.05	*g*	0.92 ± 0.07	80 ± 60[h]
Thr 73	0.66 ± 0.06	18 ± 8[f]	●		0.86 ± 0.04		0.80 ± 0.20	1000 ± 900[f]
Tyr 74	0.71 ± 0.06	13 ± 9[f]	0.71 ± 0.06	13 ± 9[f]	0.94 ± 0.05	*g*	0.90 ± 0.07	*g*
Ile 75	1.00 ± 0.05		0.76 ± 0.06	*g*	1.00 ± 0.05	*g*	0.88 ± 0.05	*g*
*Gly 77	0.76 ± 0.06	*g*	0.76 ± 0.06	*g*	●		●	
*Glu 78	0.67 ± 0.06	*g*	0.67 ± 0.06	*g*	0.74 ± 0.05		0.74 ± 0.05	
*Leu 79	●		●		0.87 ± 0.05	50 ± 35[f]	0.87 ± 0.05	50 ± 35[f]
*His 80	0.80 ± 0.06	*g*	0.80 ± 0.06	*g*	0.95 ± 0.05		0.95 ± 0.05	
*Asp 82	0.82 ± 0.05		0.82 ± 0.05		0.84 ± 0.04		0.84 ± 0.04	
*Asp 83	0.99 ± 0.05		0.99 ± 0.05		0.91 ± 0.05	*g*	0.91 ± 0.05	*g*
*Arg 84	0.92 ± 0.05		0.92 ± 0.05		0.73 ± 0.04	160 ± 60[f]	0.73 ± 0.04	160 ± 60[f]

Table 2 Continued

	2 M GdmCl				native			
	A form[b]		B form[b]		A form[b]		B form[b]	
residue[a]	S^{2c}	$\tau_e{}^d$ (ps)	S^{2c}	$\tau_e{}^d$ (ps)	S^{2c}	$\tau_e{}^d$ (ps)	S^{2c}	$\tau_e{}^d$ (ps)
*Lys 86	0.72 ± 0.05		0.72 ± 0.05		▼		▼	
*Ile 87	▼		▼		0.84 ± 0.03	300 ± 300^h	0.84 ± 0.03	300 ± 300^h
*Lys 89	▼		▼		0.91 ± 0.05		0.91 ± 0.05	
*Glu 92	▼		▼		0.58 ± 0.05	116 ± 36^h	0.58 ± 0.05	116 ± 36^h
*Leu 94	0.44 ± 0.04	50 ± 10^h	0.44 ± 0.04	50 ± 10^h	▼		▼	

[a] Single asterisk (*) denotes residues with degenerate resonances for both species. [b] (▼) Amide backbone nitrogens for which relaxation rates could not be measured due to cross-peak overlap with other resonances. [c] (●) For these residues, the Model-Free approach does not provide self-consistent results. [d] τ_e indicates either τ_f if models 2−4 are used or τ_s if model 5 is used for fitting the experimental data. [e] The relaxation rate of this residue is fitted using model 5. [f] The relaxation rate of this residue is fitted using model 4. [g] The relaxation rate of this residue is fitted using model 3. [h] The relaxation rate of this residue is fitted using model 2.

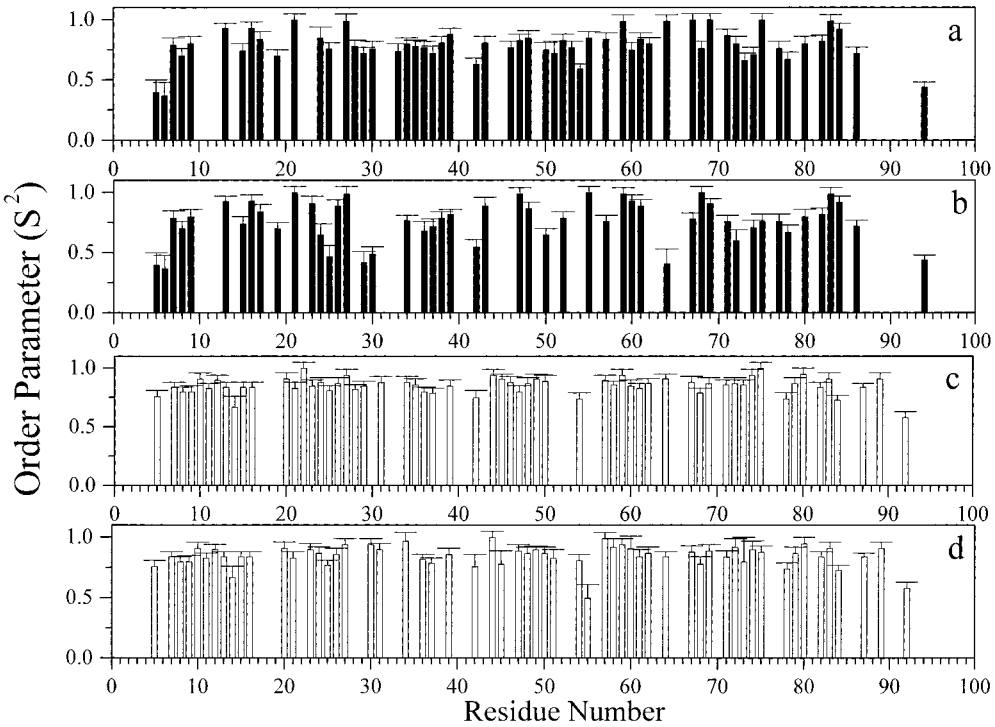

FIGURE 4: Order parameters (S^2) of the backbone nitrogens for the oxidized rat microsomal cyt b_5 in the presence of 2 M GdmCl [panels a (A form) and b (B form)] and for the native system [panels c (A form) and d (B form)].

the C-terminus, three common residues (5, 6, and 78), three residues unique for the A form (42, 54, and 73), and nine for the B form (24, 25, 29, 30, 36, 42, 50, 64, and 72) display S^2 values below 0.70, thus indicating the occurrence of extensive unfolding processes. Most of the residues experience fast librations (model 2, see Materials and Methods), while only a few residues, scattered over the protein frame, show slower internal motions (model 5). All the residues [except one for the A form (Ser 64)] displaying a dependence of the $R_{1\rho}{}^{OFF,cor}$ values with the effective magnetic field are fitted, within the Model-Free analysis, with an R_{ex} contribution to R_2 (models 3 and 4). For Ser 64 in the A form, the R_{ex} contribution is relatively small and within the error of R_2, and therefore it may easily escape from the Model-Free analysis. Furthermore, the Model-Free analysis requires the R_{ex} contribution for a few residues for which no effective field dependence has been detected, thus indicating the presence of chemical exchange processes occurring at rates faster than those accessible with the present experimental conditions.

The average S^2 values for all the characterized residues are 0.79 ± 0.14 for the A form and 0.76 ± 0.18 for the B form. These values are lower than those found in the native protein (see below), which are 0.86 ± 0.07 and 0.85 ± 0.09 for A and B forms, respectively. Therefore, it is evident that nearly the same, relatively small, change is observed for internal mobility in both the A and B forms upon addition of denaturant. A pictorial representation of these results is shown in Figure 5 for the A form (panel a) and for the B form (panel c).

Relaxation Properties of the Native, Oxidized Forms. For both the A (*20*) and the B (*18*) forms of the oxidized native state of cyt b_5, $R_{1\rho}{}^{OFF,cor}$ measurements are already available. Their values and their dependence on the effective magnetic field indicated the presence of motions in the milli- to microsecond time range on some residues in relevant regions of the protein. To complete the characterization of the motions of cyt b_5 also in the native state, ^{15}N longitudinal and transverse relaxation rates as well as heteronuclear NOEs are needed. These values recently appeared in the literature

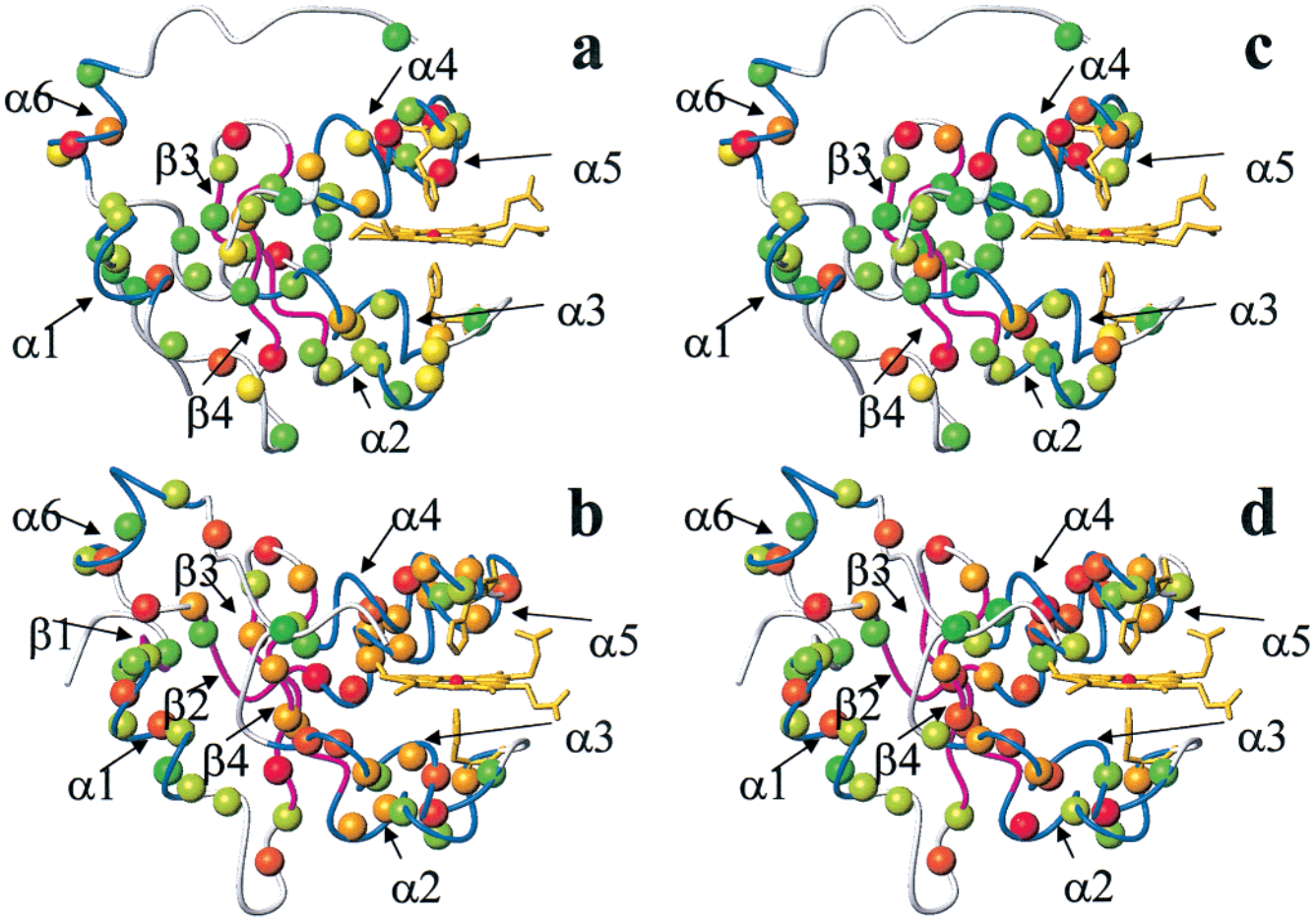

FIGURE 5: Mapping of HN mobility in the nano- to picosecond time scale in the protein frame of the A form of cyt b_5 in 2 M GdmCl (a) and in the native state (b) and of the B form of cyt b_5 in 2 M GdmCl (c) and in the native state (d). The color scale of the spheres red → yellow → green indicates increasing mobility (lower S^2 values). Secondary structure elements are indicated: α-helices in blue and β-strands in magenta.

from another laboratory (*21*); however, the measurements have been also performed within this work for consistency of the sample and experimental conditions, allowing us to make a meaningful comparison with those obtained in the presence of denaturant.

The experimental values of R_2, R_1, and heteronuclear NOEs for the native form are reported in the Supporting Information. From a Model-Free analysis of these data, performed with the same approach used for the protein in the presence of denaturant, the order parameters and the correlation times for the internal motions can be determined. The pattern of S^2 values on the protein frame is shown in Figure 5 (panels b and d).

The S^2 values of the native oxidized A and B forms display a quite more even distribution along the amino acid sequence with respect to the values in the presence of denaturant. They are reported in Table 2 and plotted in Figure 4 as well. Their values are consistent with those already reported (*21*).

Having now available the experimental R_2 values, we have reanalyzed the $R_{1\rho}^{OFF,cor}$ values, previously determined (*20*), by using the R_2 values as the $R_{1\rho}^{OFF,cor}$ limits at zero effective magnetic field. From the fitting to eq 3, now we obtain more accurate values for τ_{ex}, which are reported in Table 1. The data obviously provide the same picture in terms of exchange conformation equilibria as the previous ones. The pattern of conformational exchange processes for both forms is reported in Figure 3 (panels b and d). The correspondence between detection of exchange conformational processes determined through the Model-Free analysis and through rotating-frame experiments is essentially complete. Discrepancies observed for residues 22, 34, 45, and 49 for the A form; residues 44, 57, 58, 67, and 72 for the B form; and residue 80 unique for the two forms can be accounted on the same basis as discussed for the GdmCl system.

DISCUSSION

Cyt b_5 is now quite well-characterized in terms of mobility both on milli- to microsecond and nano- to picosecond time scales. The system is complicated by the presence of the two A and B conformers, which, however, add further pieces of information to the knowledge of the system. When the signals of the two forms are well separated, specific mobility data are available. This happens for about 40% of the signals. For the remaining signals, degenerate for the two species, the mobility parameters may be assumed to be equal for both species, as degenerate signals both in ^{1}H and ^{15}N dimensions are indicators of very similar behavior.

GdmCl changes the mobility parameters, often by increasing the internal mobility but sometimes by decreasing it. The increase in mobility can be associated to a break in the hydrogen bonds, as observed in the case of Ser 64, whereas the decrease in mobility may be related to strong interactions with the denaturant molecules.

We are now going to compare the dynamical properties of oxidized cyt b_5 in the presence or in the absence of denaturant and between A and B forms. The aim is that of providing a picture of the events occurring before the release of the heme moiety and the subsequent unfolding of the protein.

Comparison of the Dynamical Properties of cyt b_5 in 2 M GdmCl with Those of the Native State. (1) A Form. Comparing the conformational exchange processes on the milli- to microsecond time scale of the oxidized A form of cyt b_5 in the presence of 2 M GdmCl with those of the native protein (*20*) (see Table 1), the first observation to be made is that the total number of backbone nitrogens participating in exchange processes is somewhat reduced: 16 backbone nitrogens in the present system versus 28 in the native protein. The comparison includes both the resolved (10 in 2 M GdmCl and 20 in the native protein) and those coincident with those of the B form, even if for some residues the corresponding signal in both forms is not available. The decrease in number of residues experiencing conformational exchange can be due to either a $\delta\Omega$ of eq 2 that accidentally becomes close to zero upon addition of denaturant or due to the actual rigidity of the molecule. As this behavior is observed for several residues, we suggest that this is due to the real rigidity. For those residues for which the exchange process is observed, exchange rates in GdmCl are faster than in the native state. Analyzing the secondary structural elements to which they belong (see Table 1) the following major conclusions can be reached (see also Figure 3):

(i) Helix α1 (residues 9−10) is rigidified upon addition of denaturant.

(ii) Helices α2, α3, and α4 do not experience any significant change in their overall milli- to microsecond time scale backbone dynamics. For example, for helix α2 the decrease in mobility of residues 34 and 39 is partly counterbalanced by the increased mobility of Thr 33.

(iii) In helix α5 (residues 64−74 in the native form), the number of residues experiencing backbone exchange processes upon addition of 2 M GdmCl is slightly increased: three backbone NHs are now involved in exchange processes (64, 68, and 71), while two seem to be rigidified (67 and 72). It is worth noting that in the present system, helix α5 extends between residues 64−72, and it is thus shortened by residues 73 and 74 (*19*). Furthermore, extensive rearrangements in the hydrogen bond network involve its residues. This indicates that the addition of denaturant increases conformational exchange processes in protein segments where also significant structural changes are occurring.

(iv) The largest structural changes induced by the denaturant involve the protein backbone segments 33−38 (helix α2), 62−64 (end of helix α4 − beginning of helix α5), and 77−78 (*19*). Interestingly, the backbone nitrogens of residues 33, 34, 64, and 78 are also subjected to mobility changes. Three of them (33, 64, and 78) become more mobile while one (34) is rigidified.

Also on a faster time scale (nano- to picosecond range), useful information is obtained. As mentioned earlier, a decrease in the order parameter S^2 corresponds to a more mobile backbone nitrogen. By comparing the two sets of order parameters (Table 2 and Figure 5), it is observed that, in the presence of 2 M GdmCl, the backbone NHs of 10 residues (seven of which unique for the A form) have S^2 values considerably lower (outside the experimental error) than the native system. On the other hand, only four backbone NHs display S^2 values larger than in the native protein. Thus, a general comment can be made that in the nano- to picosecond time scale an overall increase in the backbone mobility is induced upon addition of 2 M GdmCl, as it is also pictorially shown in Figure 5. This increase is mostly present on backbone nitrogens located in the heme vicinity. In fact, for NHs within 8 Å from the heme moiety, six such NHs (42, 46, 50, 54, 73−74) show increased nano- to picosecond mobility in the presence of denaturant, while only two (67 and 69) such NHs display reduced S^2 values in the native system.

Again, most of the residues that show enhanced internal mobility are located in protein segments experiencing the largest structural changes induced by the denaturant. However, it seems that these fast time scale motions do not have an obvious relation with the slower conformational exchange processes. A decrease in the S^2 values is observed for helix α2 (34−38), where several hydrogen bonds are broken by the denaturant. The residues at the two extremes of the various elements of secondary structure show an increased fast mobility in 2 M GdmCl. This behavior can explain the reduction in length of these elements in the structure of the A form of cyt b_5. Finally, β-strand 5−7 moves apart from the 75−78 one. Again, this occurs together with an increase in local mobility. Indeed, in this region only residue 75 remains quite ordered in 2 M GdmCl, and the analysis of the structure in the same conditions confirms that residue 75 is still part of a β-strand.

(2) B Form. Examination of Table 1, in which the two sets of results for the B form in the presence of 2 M GdmCl and in the native state are shown together, indicates that, in analogy to the A form, the number of residues showing conformational equilibria in the milli- to microsecond time scale is again somewhat reduced upon addition of denaturant: 18 backbone nitrogens in the present system versus 35 in the native protein. Also in this form, the data for the same NH in both forms are not available for all residues.

Also in this system, although the number of residues involved in conformational equilibria is reduced, the exchange rates, when measured, are invariably faster than in the native state. By taking again into account the secondary structural elements to which the residues belong (see Table 1 and Figure 3), it can be observed that helices α2, α3, and α4 become more rigid. Helix α5 experiences a behavior similar to that observed in the A form: three residues are involved in exchange process in GdmCl and not in the native state (residues 64, 68, and 71), while only one is rigidified in the denaturant (residue 72). Since the structure of the B form of oxidized cyt b_5 in 2 M GdmCl is not available, no correlation can be made between the structural and the mobility changes. However, it is interesting to draw the attention to the changes in the conformational exchange processes involving residues 34, 36 (decreased mobility), and 64 (increased mobility), which experience small but significant structural changes upon addition of 2 M GdmCl to the A form.

Analyzing the nano- to picosecond backbone dynamics of the B forms (Table 2, columns 4 and 8, and Figure 5), it appears that in the protein in the presence of denaturant 15

backbone NHs display S^2 values considerably lower (outside the experimental error) than in the native protein, while only four backbone NHs have S^2 values larger in the denaturant than in the native species. Thus, there is a considerable net increase in nano- to picosecond mobility occurring upon addition of 2 M GdmCl to the B form, similarly to that observed for the A form. This increase is mostly located in the heme vicinity also in this form. In fact, 10 NHs within 8 Å from the iron (24−25, 30, 42, 50, 57, 64, 72, and 74−75) show considerably reduced S^2 values in the presence of denaturant while only two (55 and 68) in the native system. Summarizing, in the nano- to picosecond time scale, GdmCl exerts a considerable effect resulting in a net increase of mobility in the vicinity of the heme. The dual effect seen in the milli- to microsecond time scale is present also here but at a much lesser extent.

From this analysis, it can be deduced that the chaotropic agent guanidinium chloride added in a subdenaturing concentration to oxidized cyt b_5 acts simultaneously by "fixing" some backbone atoms and by "releasing" others. This could be done via hydrogen bond breaking/making reactions, in agreement to that already reported, i.e., that GdmCl causes protein unfolding by disrupting noncovalent interactions within native protein structures (*70*) as well as that it interacts directly with the unfolded protein via multiple hydrogen bonds (*71*).

Comparison of the Backbone Dynamics of the A and B forms of cyt b_5 in the Presence of Denaturant. The comparison between the conformational exchange behavior of the two forms in the presence of denaturant (Table 1) is performed by considering only the resolved signals for the two forms. Twelve NHs participate in exchange processes in the B form, while there are 10 in the A form. The slight increase in the number of backbone nitrogens involved in mobility of the B form relative to the A form is similar to that recently observed for these two forms in the native state of the protein (*18*). More specifically, six backbone nitrogens display milli- to microsecond mobility in both forms, six solely in the B form and four solely in the A form. Most of the residues involved in conformational exchange processes are located around the heme. Four of the six residues in the B form are either in direct van der Waals contact with the heme (58 and 67) or within one bond away (26 and 75). The four backbone nitrogens that participate in exchange processes only in the A form are in direct van der Waals contact with the heme (46) or within one bond away (24, 33, and 60).

Analyzing the nano- to picosecond mobility of the two forms of oxidized cyt b_5 in the presence of denaturant (Table 2), it can be observed that nine backbone nitrogens display an increase in local mobility in the B form with respect to the A form,while four display increased local mobility in the A form. The most dramatic differences are observed for residues 25, 29−30, and 64, with Ser 64 experiencing the largest (0.99 → 0.41 in the S^2 value). Ser 64 is one of the residues whose backbone experiences a significant structural change upon addition of GdmCl in the A form (*19*), but it is not known whether this structural change occurs also in the B form. However, it can be proposed that Ser 64 is quite affected by the presence of denaturant also in this form. With respect to the secondary structure elements, it can be observed the considerable increase in local mobility for the β3 and β4 strands in the B form with respect to the A (residues 24, 25, 29, and 30). This behavior could indicate that there is an increase in internal mobility around the heme in the B form relative to the A form in 2 M GdmCl.

CONCLUSIONS

The effect of a denaturant on the A and B forms of oxidized cyt b_5 is that of slightly increasing the internal mobility both in the milli- to microsecond and the nano- to picosecond time scales. As already noted in other systems (*37*, *72*−*74*), the mobility in these two time scales is generally uncorrelated. In the present system, most of the increased mobility is concentrated around the heme group. The larger increase in mobility for both ranges of rates as well as for both forms is observed in the β-sheets and, at a smaller extent, in the α-helices that form the heme binding pocket. These regions are those that experience the largest structural changes upon addition of GdmCl to the A form of oxidized cyt b_5 (*19*). However, the effect is not as large as could have been expected. At 2.6−2.9 M concentration of GdmCl, the heme is totally released (*19*, *23*) and the protein shows NMR spectra typical of a random coil system (*19*).

It is found that, upon addition of denaturant, some residues have increased mobility while others reduced in the same secondary structure element. Helix α1 is definitely rigidified in the milli- to microsecond time range. The increased rigidity could suggest that the denaturant establishes new hydrogen bonds and stabilizes one of the conformations within which there is mobility in the native state. Helix α5 becomes more mobile, and this effect is larger in the B form than in the A form. The latter observation can be related to the slightly lower stability of the B form with respect to denaturants (by ∼7 kJ mol^{-1}).

Lower S^2 values were observed for more residues in the B form than in the A form. This may be due to the greater effect of the denaturant on the B form. Values of $S^2 < 0.7$ and long τ values (>200 ps), which are typical of partially folded systems (*26*, *32*, *75*, *76*), involve for the B form Leu 25 [which is in contact with the heme and possibly affects its orientation (*22*, *77*)] belonging to β4; Val 29 belonging to β3; Leu 36 belonging to α2; and Lys 72, which is the last residue of α5. For the A form, long τ values are found for residues Gly 42 and Gly 51 both belonging to turns. For both the A and the B forms, large mobility, as indicated by long τ values, is experienced by residues Lys 5 and Tyr 6 belonging to strand β1, which loses regular structure upon addition of denaturant. Residues 24, 30, 42, 50, and 64 in the B form, residues 54 and 73 in the A form, and residues 78 and 94, unique for the two forms, also show $S^2 < 0.7$. The regions showing increased mobility are mainly those forming the heme pocket. This mobility would facilitate the release of the heme at lower GdmCl concentration in the B form of the protein, as it is indeed observed.

To understand the relevance of the internal mobility with respect to the biological function, it is meaningful to consider the pattern of the order parameters and the distribution and rates of the exchange processes over the molecule, rather than analyzing the values of the single, individual NH. From inspection of Figures 3 and 5, it appears that the effect of addition of GdmCl is that of an overall, even if not dramatic,

increase in internal mobility. The first steps of the unfolding process involve the breaking of the hydrogen bond between the peptidic nitrogen of Ser 64 with a propionate group and the concomitant reduction of the helix α5 on the side of residues 73−74 (*19*). The following determinant step in the unfolding process is the detachment of the heme moiety followed by the obtainment of an unfolded state of the protein. Therefore, the heme cofactor represents a relevant element for the stabilization of the protein. It can be noted that the more mobile parts of the protein and those more affected by the denaturant are those around the heme. The resulting picture is essentially consistent with the data obtained in the apo form, which shows large mobility in the subnanosecond time scale in the helices and turns around the heme (*36*).

All residues (33−38, 62−64, and 77−78) that experienced structural changes in the A form of the protein upon addition of GdmCl show reduced S^2 values and, for some of them (33, 38, 64, and 78), conformational equilibria not present in the native state. Only two exceptions to the general trend of increased mobility in the nano- to picosecond time scale are shown by residues Ser 64 and Ala 67, which have an increased order parameter in the presence of denaturant. This can be rationalized taking into account that the NH of these two residues, despite the break of relevant interactions induced by the denaturant, now form new hydrogen bonds that can stabilize the new conformation (*19*).

In the present system, at variance with other partially unfolded proteins investigated, the secondary structure elements present in the native state are essentially conserved. This behavior could rationalize why the internal mobility is not significantly altered. Indeed, in an intermediate of a HiPIP from *Chromatium vinosum* in 4 M GdmCl, where secondary structure elements are lost, the mobility is dramatically increased (*35*). It can be proposed that, as long as secondary structure elements are present, the mobility is moderately affected by denaturants. Locally, if the denaturant breaks relevant hydrogen bonds, mobility is altered and can be either increased or decreased. In the former case, it is essentially as expected. In the latter case, new hydrogen bonds with the denaturant can be formed.

SUPPORTING INFORMATION AVAILABLE

Two figures depicting the off-resonance ^{15}N rotating-frame relaxation rates, $R_{1\rho}^{OFF,cor}$, of the backbone nitrogens of the A and B forms of oxidized rat microsomal cyt b_5 in the presence of 2 M GdmCl and the ^{15}N relaxation parameters, R_2, R_1, and $^1H-^{15}N$ NOEs, for both native cyt b_5 and in the presence of 2 M GdmCl (3 pages). This material is available free of charge via the Internet at http://pubs.acs.org.

REFERENCES

1. von Bodman, S. B., Schulder, M. A., Jollie, D. R., and Sligar, S. G. (1986) *Proc. Natl. Acad. Sci. U.S.A. 83*, 9443−9447.
2. Ito, A., and Sato, R. (1968) *J. Biol. Chem. 243*, 4922−4923.
3. Spatz, L., and Strittmatter, P. (1971) *Proc. Natl. Acad. Sci. U.S.A. 68*, 1042−1046.
4. Oshino, N., Imai, Y., and Sato, R. (1971) *J. Biochem. (Tokyo) 69*, 155−167.
5. Strittmatter, P., Spatz, L., Corcoran, D., Rogers, M. J., Setlow, B., and Redline, R. (1974) *Proc. Natl. Acad. Sci. U.S.A. 71*, 4565−4569.
6. Hildebrandt, A., and Estabrook, R. W. (1971) *Arch. Biochem. Biophys. 143*, 66−79.
7. Hegesh, E., Hegesh, J., and Kaftory, A. (1986) *N. Engl. J. Med. 314*, 757−761.
8. Strittmatter, P., and Ozols, J. (1966) *J. Biol. Chem. 241*, 4787−4792.
9. Keller, R. M., and Wüthrich, K. (1980) *Biochim. Biophys. Acta 621*, 204−217.
10. La Mar, G. N., Burns, P. D., Jackson, J. T., Smith, K. M., and Langry, K. C. (1981) *J. Biol. Chem. 256*, 6075−6079.
11. Lederer, F. (1994) *Biochimie 76*, 674−692.
12. Rivera, M., Barillas-Mury, C., Christensen, K. A., Little, J. W., Wells, M. A., and Walker, F. A. (1992) *Biochemistry 31*, 12233−12240.
13. Banci, L., Bertini, I., Rosato, A., and Scacchieri, S. (2000) *Eur. J. Biochem. 267*, 755−766.
14. Arnesano, F., Banci, L., Bertini, I., and Felli, I. C. (1998) *Biochemistry 37*, 173−184.
15. Durley, R. C. E., and Mathews, F. S. (1996) *Acta Crystallogr. D 52*, 65−72.
16. Muskett, F. W., Kelly, G. P., and Whitford, D. (1996) *J. Mol. Biol. 258*, 172−189.
17. Rodriguez Maranon, M. J., Qiu, F., Stark, R. E., White, S. P., Zhang, X., Foundling, S. I., Rodriguez, V., Schilling, C. L., Bunce, R. A., and Rivera, M. (1996) *Biochemistry 35*, 16378−16390.
18. Arnesano, F., Banci, L., Bertini, I., Felli, I. C., and Koulougliotis, D. (1999) *Eur. J. Biochem. 260*, 347−354.
19. Arnesano, F., Banci, L., Bertini, I., and Koulougliotis, D. (1998) *Biochemistry 37*, 17082−17092.
20. Banci, L., Bertini, I., Cavazza, C., Felli, I. C., and Koulougliotis, D. (1998) *Biochemistry 37*, 12320−12330.
21. Dangi, B., Blankman, J., Miller, C. J., Volkman, B. F., and Guiles, R. D. (1998) *J. Phys. Chem. 102*, 8201−8208.
22. Dangi, B., Sarma, S., Yan, C., Banville, D. L., and Guiles, R. D. (1998) *Biochemistry 37*, 8289−8302.
23. Tajima, S., Enomoto, K., and Sato, R. (1976) *Arch. Biochem. Biophys. 172*, 90−97.
24. Manyusa, S., Mortuza, G., and Whitford, D. (1999) *Biochemistry 38*, 14352−14362.
25. Buck, M., Schwalbe, H., and Dobson, C. M. (1995) *Biochemistry 34*, 13219−13232.
26. Barbar, E., Hare, M., Daragan, V., Barany, G., and Woodward, C. (1998) *Biochemistry 37*, 7822−7833.
27. Wong, K. B., Freund, S. M. V., and Fersht, A. R. (1996) *J. Mol. Biol. 259*, 805−818.
28. Shortle, D. R. (1996) *Curr. Opin. Struct. Biol. 6*, 24−30.
29. Dyson, H. J., and Wright, P. E. (1998) *Nat. Struct. Biol. 5*, 499−503.
30. Szyperski, T., Luginbuhl, P., Otting, G., Güntert, P., and Wüthrich, K. (1993) *J. Biomol. NMR 3*, 151−164.
31. Redfield, C., Smith, R. A. G., and Dobson, C. M. (1994) *Nat. Struct. Biol. 1*, 23−29.
32. Buck, M., Schwalbe, H., and Dobson, C. M. (1996) *J. Mol. Biol. 257*, 669−683.
33. Natarajan, K., and Cowan, J. A. (1997) *J. Am. Chem. Soc. 119*, 4082−4083.
34. Bian, S., and Cowan, J. A. (1998) *J. Am. Chem. Soc. 120*, 3532−3533.
35. Bentrop, D., Bertini, I., Iacoviello, R., Luchinat, C., Niikura, Y., Piccioli, M., Presenti, C., and Rosato, A. (1999) *Biochemistry 38*, 4669−4680.
36. Bhattacharya, S., Falzone, C. J., and Lecomte, J. T. J. (1999) *Biochemistry 38*, 2577−2589.
37. Zinn-Justin, S., Berthault, P., Guenneugues, M., and Desvaux, H. (1997) *J. Biomol. NMR 10*, 363−372.
38. Desvaux, H., Berthault, P., Birlirakis, N., Goldman, M., and Piotto, M. (1995) *J. Magn. Reson. 113*, 47−52.
39. Shaka, A. J., Keeler, J., and Freeman, R. (1983) *J. Magn. Reson. 53*, 313−340.
40. Morris, G. A., and Freeman, R. (1979) *J. Am. Chem. Soc. 101*, 760−762.
41. Marion, D., and Wüthrich, K. (1983) *Biochem. Biophys. Res. Commun. 113*, 967−974.

42. Peng, J. W., and Wagner, G. (1994) *Methods Enzymol. 239*, 563−596.
43. Kay, L. E., Nicholson, L. K., Delaglio, F., Bax, A., and Torchia, D. A. (1992) *J. Magn. Reson. 97*, 359−375.
44. Grzesiek, S., and Bax, A. (1993) *J. Am. Chem. Soc. 115*, 12593−12594.
45. Guiles, R. D., Basus, V. J., Sarma, S., Malpure, S., Fox, K. M., Kuntz, I. D., and Waskell, L. (1993) *Biochemistry 32*, 8329−8340.
46. Marquardt, D. W. (1963) *J. Soc. Ind. Appl. Math. 11*, 431−441.
47. Press, W. H., Flannery, B. P., Teukolsky, S. A., and Vetterling, W. T. (1988) *Numerical Recipes in C: The Art of Scientific Computing*, Cambridge University Press, New York.
48. Palmer, A. G., III, Rance, M., and Wright, P. E. (1991) *J. Am. Chem. Soc. 113*, 4371−4380.
49. Peng, J. W., and Wagner, G. (1992) *Biochemistry 31*, 8571−8586.
50. James, T. L., Matson, G. B., Kuntz, I. D., and Fisher, R. W. (1977) *J. Magn. Reson. 28*, 417−426.
51. Davis, D. G., Perlman, M. E., and London, R. E. (1994) *J. Magn. Reson. Ser. B 104*, 266−275.
52. Desvaux, H., Birlirakis, N., Wary, C., and Berthault, P. (1995) *Mol. Phys. 86*, 1059−1073.
53. Akke, M., and Palmer, A. G., III. (1996) *J. Am. Chem. Soc. 118*, 911−912.
54. Mandel, M. A., Akke, M., and Palmer, A. G., III. (1995) *J. Mol. Biol. 246*, 144−163.
55. Lipari, G., and Szabo, A. (1982) *J. Am. Chem. Soc. 104*, 4546−4559.
56. Abragam, A. (1961) *The Principles of Nuclear Magnetism*, Oxford University Press, Oxford.
57. Clore, G. M., Szabo, A., Bax, A., Kay, L. E., Driscoll, P. C., and Gronenborn, A. M. (1990) *J. Am. Chem. Soc. 112*, 4989−4991.
58. Schurr, J. M., Babcock, H. P., and Fujimoto, B. S. (1994) *J. Magn. Reson. Ser. B 105*, 211−224.
59. Tjandra, N., Wingfield, P., Stahl, S., and Bax, A. (1996) *J. Biomol. NMR 8*, 273−284.
60. Luginbuhl, P., Pervushin, K. V., Iwai, H., and Wüthrich, K. (1997) *Biochemistry 36*, 7305−7312.
61. Woessner, D. E. (1962) *J. Chem. Phys. 3*, 647−652.
62. Halle, B., and Wennerström, H. (1981) *J. Phys. Chem. 75*, 1928−1943.
63. Barbato, G., Ikura, M., Kay, L. E., Pastor, R. W., and Bax, A. (1992) *Biochemistry 31*, 5269−5278.
64. Banci, L., Felli, I. C., and Koulougliotis, D. (1998) *J. Biomol. NMR 12*, 307−318.
65. Santoro, M. M., and Bolen, D. W. (1988) *Biochemistry 27*, 8063−8068.
66. Agashe, V. R., and Udgaonkar, J. B. (1995) *Biochemistry 34*, 3286−3299.
67. Bhuyan, A. K., and Udgaonkar, J. B. (1998) *Biochemistry 37*, 9147−9155.
68. Walker, F. A., Emrick, D., Rivera, J. E., Hanquet, B. J., and Buttlaire, D. H. (1988) *J. Am. Chem. Soc. 110*, 6234−6240.
69. Tjandra, N., Feller, S. E., Pastor, R. W., and Bax, A. (1995) *J. Am. Chem. Soc. 117*, 12562−12566.
70. Matthews, C. R. (1993) *Annu. Rev. Biochem. 62*, 653−683.
71. Makhatadze, G. I., and Privalov, P. L. (1992) *J. Mol. Biol. 226*, 491−505.
72. Mandel, M. A., Akke, M., and Palmer, A. G., III. (1996) *Biochemistry 35*, 16009−16023.
73. Tjandra, N., Kuboniwa, H., Ren, H., and Bax, A. (1995) *Eur. J. Biochem. 230*, 1014−1024.
74. Habazettl, J., Myers, C., Yuan, F., Verdine, G., and Wagner, G. (1996) *Biochemistry 35*, 9335−9348.
75. Alexandrescu, A. T., Abeygunawardana, C., and Shortle, D. (1994) *Biochemistry 33*, 1063−1072.
76. Brutscher, B., Brüschweiler, R., and Ernst, R. R. (1997) *Biochemistry 36*, 13043−13053.
77. Mortuza, G. B., and Whitford, D. (1997) *FEBS Lett. 412*, 610−614.

BI992756K